8-1-2013

Changes in Elastic Wave Velocity and Rock Microstructure Due to Basalt-CO_2-Water Reactions

Ludmila Adam
University of Auckland

Kasper van Wijk
University of Auckland

Thomas Otheim
Boise State University

Michael Batzle
Colorado School of Mines

Changes in elastic wave velocity and rock microstructure due to basalt-CO$_2$-water reactions

Ludmila Adam,[1] Kasper van Wijk,[2] Thomas Otheim,[3] and Michael Batzle[4]

[1] The chemical interaction between carbon dioxide, water, and basalt is a common process in the earth, which results in the dissolution of primary minerals that later precipitate as alteration minerals. This occurs naturally in volcanic settings, but more recently basalts have been suggested as reservoirs for sequestration of anthropogenic CO$_2$. In both the natural and man-made cases, rock-fluid reactions lead to the precipitation of carbonates. Here, we quantify changes in ultrasonic wave speeds, associated with changes in the frame of whole-rock basalts, as CO$_2$ and basalt react. After 30 weeks of reactions and carbonate precipitation, the ultrasonic wave speed in dry basalt samples increases between 4% and 20% and permeability is reduced by up to an order of magnitude. However, porosity decreases only by 2% to 3%. The correlation between significant changes in wave speed and permeability indicates that a precipitate is developing in fractures and compliant pores. Thin sections, XRF-loss on ignition, and water chemistry confirm this observation. This means time-lapse seismic monitoring of a CO$_2$-water-basalt system cannot assume invariance of the rock frame, as typically done in fluid substitution models. We conclude that secondary mineral precipitation causes a measurable change in the velocities of elastic waves in basalt-water-CO$_2$ systems, suggesting that seismic waves could be used to remotely monitor future CO$_2$ injection sites. Although monitoring these reactions in the field with seismic waves might be complicated due to the heterogeneous nature of basalt, quantifying the elastic velocity changes associated with rock alteration in a controlled laboratory experiment forms an important step toward field-scale seismic monitoring.

Citation: Adam, L., K. van Wijk, T. Otheim, and M. Batzle (2013), Changes in elastic wave velocity and rock microstructure due to basalt-CO$_2$-water reactions, *J. Geophys. Res. Solid Earth*, *118*, 4039–4047, doi:10.1002/jgrb.50302.

1. Introduction

[2] Carbon dioxide (CO$_2$) naturally occurs in many geological environments, creating hydrothermal rock alterations. These rock-fluid interactions play a role in volcano edifice stability [*Lopez and Williams*, 1993; *Reid et al.*, 2001], the rupture of fluid conducting faults [*Bruhn et al.*, 1994; *Caine et al.*, 2010], and hydrothermal venting in subsea basalts [*Goldberg*, 2011; *Kelley et al.*, 2001]. In addition, rock alterations on Mars have been suggested to result from geochemical reactions between CO$_2$, water, and basalts [*Romanek et al.*, 1994; *Baker et al.*, 2000].

[3] Anthropogenic CO$_2$ injected in subsurface geologic reservoirs also creates rock-fluid reactive processes. Geologic sequestration of CO$_2$ in sedimentary geologic reservoirs has been proposed as one way to minimize the emission of this greenhouse gas [*Bachu*, 2003; *Torp and Gale*, 2004; *Benson and Cole*, 2008]. Although not always thought of as a reservoir rock, basalts may be an attractive candidate to sequester CO$_2$ in the subsurface, because of their CO$_2$-trapping potential and their massive and worldwide presence [*Bachu et al.*, 1994; *McGrail et al.*, 2006; *Oelkers et al.*, 2008; *Matter and Kelemen*, 2009].

[4] The storage capacity of CO$_2$ in basalt is largely concentrated in the top- and bottom-flow units, where the rock is brecciated and composed of large vesicles and fractures that result in rock porosity of 15% or more [*McGrail et al.*, 2006]. Inner flows cool slower and hence provide denser and impermeable layers to potentially trap injected CO$_2$. Pilot programs are under way to test geologic sequestration of CO$_2$ in the Columbia River Basalts [*McGrail et al.*, 2011] and at the Hellisheidi geothermal power plant in Iceland [*Gislason et al.*, 2010]. Proposed methods to monitor the rock-fluid interactions in basalt reservoirs include water chemistry analysis and tracer tests but do not include seismic methods [*Gislason et al.*, 2010]. Here we test the feasibility

[1] School of Environment and IESE, University of Auckland, Auckland, New Zealand.
[2] Department of Physics, University of Auckland, Auckland, New Zealand.
[3] Department of Geosciences, Boise State University, Boise, Idaho, USA.
[4] Department of Geophysics, Colorado School of Mines, Golden, Colorado, USA.

Corresponding author: L. Adam, University of Auckland, Science Center, 23 Symonds St., Auckland, 1142, New Zealand. (l.adam@auckland.ac.nz)

Table 1. Helium Permeability From 0 to 30 Weeks of Reactions (k_0 and k_{30}, Respectively, in 10^{-16} m^2), Porosity (ϕ), and Average P and S Wave Velocity Changes (ΔV_P and ΔV_S, Respectively) From 0 to 30 Weeks[a]

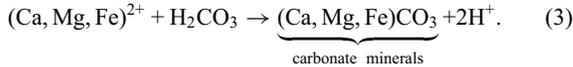| Sample	k_0	k_{30}	ϕ_0 (%)	ϕ_{30} (%)	ΔV_P (%)	ΔV_S (%)
B1	11.16	3.11	18.08	17.28	13	3.1
B2	1.45	N/M	13.52	N/M	9	3.1
B3	11.72	0.94	15.16	13.03	22	3.3

[a]Helium and porosity measurements were performed with a confining pressure of 17.2 MPa. N/M means no measurable fluid flow.

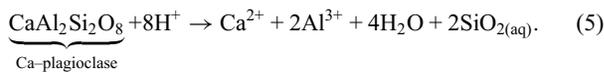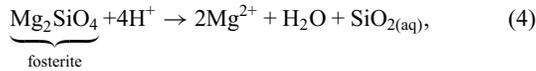of monitoring changes in rock microstructure with elastic waves on basalt cores exposed to CO_2.

[5] The minerals in basalts have the highest dissolution rate of igneous rocks when exposed to CO_2, because this rate increases as the silica-oxygen ratio content in minerals decreases [*Wolff-Boenisch et al.*, 2006]. Carbonic acid is the combination of carbon dioxide and water and dissociates into bicarbonate and hydrogen:

$$CO_2 + H_2O \rightleftharpoons H_2CO_3, \quad (1)$$

$$H_2CO_3 \rightleftharpoons HCO_3^- + H^+. \quad (2)$$
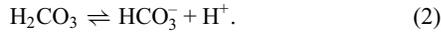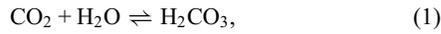
The water-CO_2 solution interacts with basalts, leaching divalent metal cations into the aqueous solution. These cations react with CO_2 and H_2O and precipitate as carbonates [*Schaef and McGrail*, 2009; *Oelkers et al.*, 2008; *Gislason et al.*, 2010]:

$$(Ca, Mg, Fe)^{2+} + H_2CO_3 \rightarrow \underbrace{(Ca, Mg, Fe)CO_3}_{\text{carbonate minerals}} + 2H^+. \quad (3)$$

[6] The reaction in equation (3) shows that for every mole of carbonate precipitated, two moles of H^+ ions are produced [*Matter and Kelemen*, 2009]. For this reaction to progress, the released H^+ ions have to be consumed by a coupled reaction. Basalt mineral dissolution reactions intake these hydrogen ions, dissolving new metal cations and increasing their concentration in the reservoir water [*Matter and Kelemen*, 2009; *Gislason et al.*, 2010; *Gislason and Hans*, 1987; *Matter et al.*, 2007]. The following equations show two of several reactive basalt minerals consuming available hydrogen ions and releasing new divalent metal cations into the water:

$$\underbrace{Mg_2SiO_4}_{\text{fosterite}} + 4H^+ \rightarrow 2Mg^{2+} + H_2O + SiO_{2(aq)}, \quad (4)$$

$$\underbrace{CaAl_2Si_2O_8}_{\text{Ca–plagioclase}} + 8H^+ \rightarrow Ca^{2+} + 2Al^{3+} + 4H_2O + 2SiO_{2(aq)}. \quad (5)$$

[7] These dissolved cations will then react with the CO_2-water mixture (equation (3)) to precipitate as carbonates. With newly available metal cations and the consumption of hydrogen ions in dissolution processes, carbonate precipitation can proceed in this reactive cycle. Sources for rapidly dissolvable divalent cations in basalts are olivine, plagioclase, glass, pyroxene, and serpentine [*Oelkers et al.*, 2008; *Matter and Kelemen*, 2009], and thus detailed sample characterization is important in CO_2 reactive studies.

[8] Several factors will control the dissolution of basalt minerals. For example for volcanic glass, dissolution will increase if the solution pH decreases and temperature increases [*Gislason and Oelkers*, 2003]. Thus far, experiments on carbonic acid-basalt reactivity have principally focused on water chemistry and the geochemistry in crushed samples to understand the factors that control the dissolution of basalt minerals and carbonate precipitation [*Gislason and Hans*, 1987; *Baker et al.*, 2000; *McGrail et al.*, 2006; *Matter et al.*, 2007; *Matter and Kelemen*, 2009; *Giammar et al.*, 2005; *Schaef et al.*, 2010]. But to our knowledge, no studies to date address changes to the geophysical and petrographic properties as a result of these processes in whole-rock basalts.

[9] Imaging basalts in the field has been performed with P and S wave passive seismic tomography of volcanoes [*Zandomeneghi et al.*, 2009; *Vanorio et al.*, 2005] and with vertical seismic profiles [*Pujol and Smithson*, 1991; *Eaton et al.*, 1996] or cross-well geometries [*Daley et al.*, 2004], but seismic monitoring in basalt environments is rare, as are laboratory data to monitor fluid substitution in basalts [*Johnston and Christensen*, 1997; *Vanorio et al.*, 2002; *Adelinet et al.*, 2010; *Adam and Otheim*, 2013]. Elastic waves have been used to quantify fluid substitution in sedimentary basins [*Arts et al.*, 2004; *Landrø*, 2001; *Tura and Lumley*, 1998] and rock-CO_2 reactions in carbonates and sandstones [*Vialle and Vanorio*, 2011; *Joy et al.*, 2011], but an integrated laboratory experiment to monitor CO_2-basalt reactivity with ultrasonic waves is a first and necessary step toward field-scale monitoring of these rock-fluid interactions. We present time-lapse elastic waveforms on dry laboratory samples after controlled reactions of CO_2-water-basalt to analyze potential changes to the rock frame. By quantifying the changes in seismic velocity due to rock alteration, we discuss its implications when interpreting time-lapse seismic changes and the feasibility of seismic monitoring for CO_2 sequestration in basalts.

2. Sample Characterization

[10] Three whole-rock samples were collected from outcrops corresponding to top-flow units in a basalt sequence in the Western Snake River Plain near Hagerman, Idaho [*Adam and Otheim*, 2013]. These rocks were cored to cylinders of 2.5 cm in diameter and 3.8 cm in length and named samples B1, B2, and B3. Visually, samples B1 and B3 appear different from B2, but an X-ray fluorescence (XRF) analysis shows the three rocks are nearly identical in chemical composition and all classified as ferro-basalts, with an iron oxide (Fe_2O_3) content greater than 16%. The porosity and permeability of these samples range from 15.2% to 18.1% and 1.45 to 11.72×10^{-16} m^2, respectively (Table 1), values that are in agreement with other vesicular basalt studies [*Saar and Manga*, 1999].

[11] Thin sections of the three basalt samples (left panels of Figure 1) show an average 15% olivine volumetric mineral composition and at least 31% of plagioclase. Samples B1 and B3 have 50% groundmass (glass and smaller olivine, pyroxene crystals), while sample B2 has no glass but a 15% pyroxene composition. All samples have phenocrysts of similar size, but the vesicle size is greater for sample B1 and B3 compared to B2. Therefore, sample B2 most likely stems from the interior of a porphyritic lava flow, and the phenocrysts in samples B1 and B3 nucleated prior to ascending to the surface. The volumetric mineral composition is
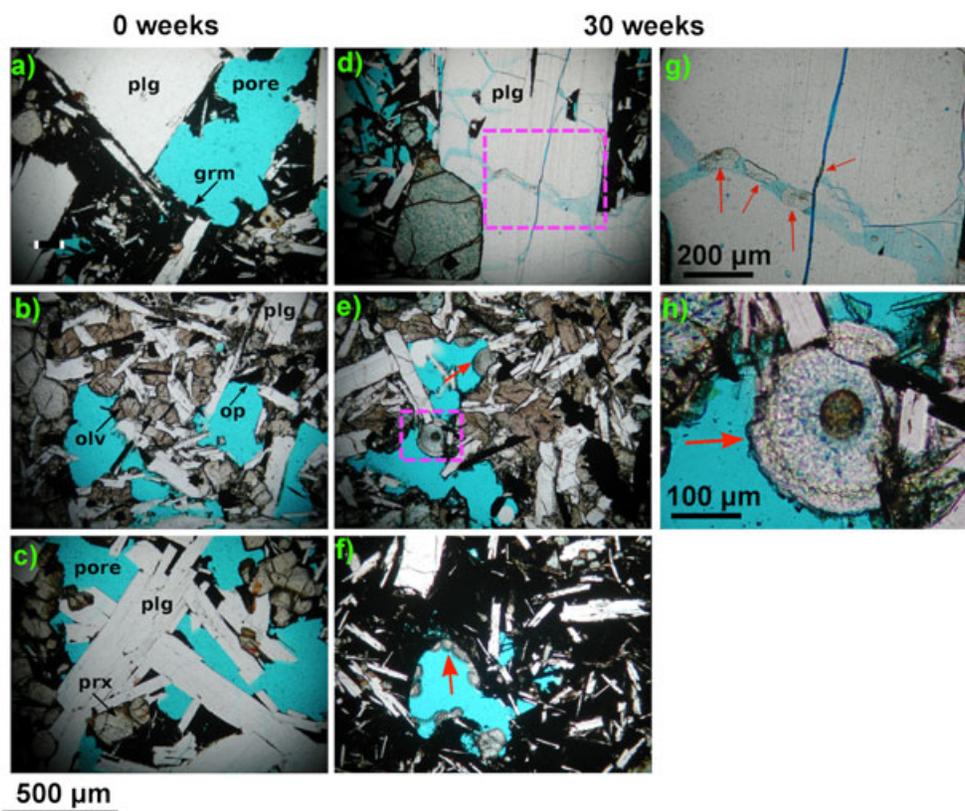
Figure 1. Thin sections of basalt samples before and after CO_2-basalt reactions. (a–c) Samples B1, B2, and B3 (respectively) before reactions (0 week) where carbonates are not observed. (d–h) After 30 weeks of reactions, rounded (botryoidal) carbonate precipitate lines the pore space and fills fractures. Figures 1d, 1e, and 1f are samples B1, B2, and B3, respectively. Figures 1g and 1h are zooms of the boxed areas where fractures and compliant pores show carbonate precipitate. Arrows point at the precipitate. The blue color represents epoxy filling the pore space (pore); plg is plagioclase, olv is olivine, prx is pyroxene, grm is groundmass, and op is opaque minerals.

estimated from thin sections and an X-ray diffraction (XRD) analysis (Table 2). While both of these methods only sample a small area or volume of the rock, computerized tomography (CT) scanning provides a nondestructive method to image the bulk structure of rocks. Figure 2 contains slices of the CT data with a maximum resolution of $\sim$ 40 μm. The gray scale is proportional to density. Sequential slices and 3-D renderings determined that the pores in these samples range from almost perfectly spherical vesicles to compliant pores and cracks. The panels on the right were acquired at double the pixel resolution of the panels on the left. To better compare the CT images, we performed pixel smoothing to the data on the right column. Nonetheless, after this processing, the images are not identical in sample location and resolution, which prevents us from direct subtraction of CT scans before and after reactions.

3. Experimental Design

[12] In the preparation of CO_2 sequestration of our samples in the presence of formation-resembling water, tap water is equilibrated with crushed basalt (50 g of crushed basalt in 200 mL of tap water) for a period of 2 weeks. After that, samples are placed in a stainless-steel vessel and evacuated to remove air. We add 60 mL of the basalt-equilibrated water to the vessel and then flood the chamber with 14.6 g of CO_2, creating a mixture at 3.5 mol/L concentration. Pressure and temperature conditions in the vessel are 8.3 MPa and 100 °C, respectively, representative of the fluid pressure and temperature in a basalt reservoir in Idaho at 1 km depth. These parameters are fixed throughout the 30 weeks of the experiment. Under these conditions, the CO_2 is in supercritical condition, where the fluid has the viscosity of a gas but a density of a liquid. The temperature and pressure conditions for this CO_2 phase are also important to ensure that in these basalts, carbonates precipitate in greater volume than clays and zeolites, which do not consume the carbon in CO_2 [*Gislason et al.*, 2010].

Table 2. The Mineralogical Rock Composition Based on XRD Measurements Show a Significant Similarity Between the Three Samples

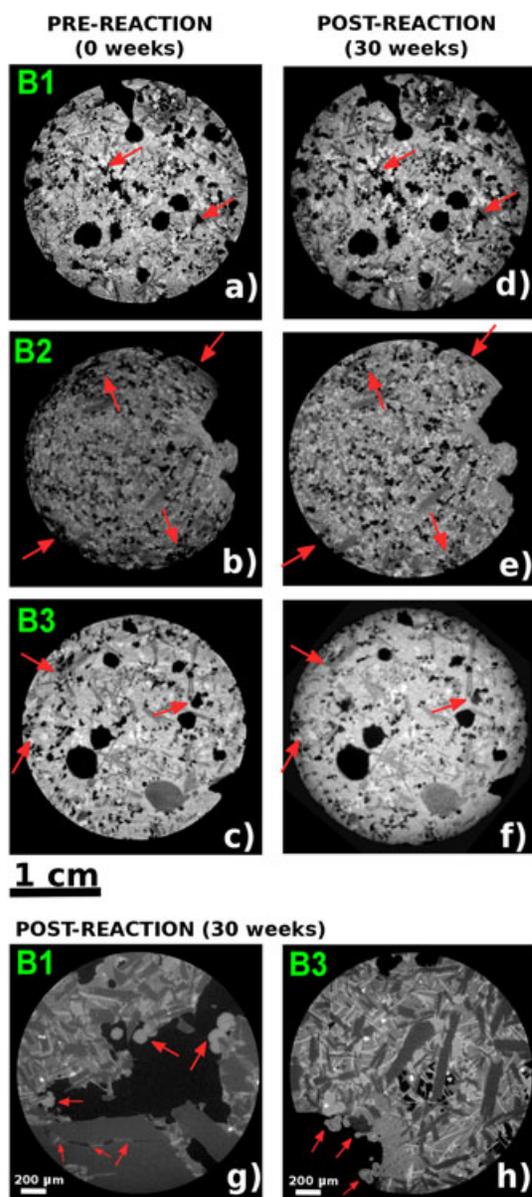| Sample/Minerals	B1	B2	B3
Plagioclase %	62.7	67.3	66.3
Pyroxene %	19.3	15.1	13
Olivine %	13.8	12.2	15.5
Gypsum %	1.7	.7	.6
Ilmenite %	2.5	4.7	4.6
Total %	100	100	100

Figure 2. Computerized tomography (CT) scan images of basalt samples (a–c) before and (d–f) after CO_2-basalt reactivity. The top panels are sample B1, middle panels are sample B2, and the bottom panels are sample B3. The gray scale is proportional to density, where mineral density increases from dark to light. Black represents the pore space, the lightest grays correlate with the higher density of olivine and pyroxene, and less-dense plagioclase is represented by a darker gray. These data are presented to show that by imaging the basalts as a whole, the precipitation of carbonates is not observed in large volumes (e.g., completely filling pore spaces). Arrows point at some of the areas in the samples where we can interpret mineral precipitation. Figures 2g and 2h are CT images at higher magnification where arrows point at botryoidal carbonate texture in pores and cracks.

[13] The samples were taken out of the vessel after 15 weeks and oven dried at 50°C before recording ultrasonic waveforms again. These steps were then repeated for a second 15 week sequestration experiment. Water extracted from the vessel at 15 and 30 weeks is compared to a baseline solution by analyzing element concentration with an inductively coupled plasma-mass spectrometer. A high-pressure pH probe monitored the pH of the water-CO_2 mixture from 0 to 13 weeks.

[14] Rock petrography and geochemistry are analyzed before and after the 30 weeks of the experiment. These include XRF, XRD, thin sections, CT scans, porosity, and permeability measurements. These data are integrated with the time-lapse elastic wave measurements to monitor carbonate precipitation in basalts in the presence of carbonic acid.

4. Time-Lapse Measurements of the Elastic Wave Field

[15] Elastic waveforms are recorded on dry samples at room conditions to study the changes to the rock frame after basalt and CO_2 have reacted. The first measurement on the samples before any reactions are induced is our baseline, or 0 week data. The elastic wave speed in these three basalts is estimated with a laser-ultrasonic system, where waves are excited by thermoelastic expansion of a 10 ns laser pulse focused on a subcentimeter area and detected by a scanning laser interferometer with a $\sim 50 \, \mu m$ spot size [*Blum et al.*, 2010]. For each sample, the source location is fixed at 1.7 cm from the sample edge, and we scan the full length of the core in transmission mode (Figure 3a). With this nondestructive and noncontacting experimental setup, the receiver laser records the wave field (absolute particle velocity) along the samples at 0.245 mm increments, averaging 256 times for each wave form, for a total of 144 traces for each sample and reaction time interval. The dominant frequency of the ultrasonic waves is 0.5 MHz. The target of this study is to quantify changes to the frame of the basalts (i.e., dry rock) as rock-fluid interactions develop. Because the elastic wave velocity in dry rocks does not depend on frequency, our velocity observations at ultrasonic frequencies can potentially be used in the analysis of active seismic surveys frequencies (5–100 Hz).

[16] The top panel of Figure 3 depicts the experimental geometry, while subsequent panels represent the wave fields detected after 0, 15, and 30 weeks of rock-fluid interactions at in situ conditions. The variability in these measurements displays that these rocks are strongly heterogeneous. The travel time of the first arriving energy corresponding to the compressional (*P*) wave is picked at each reaction time interval, for all wave forms and all samples. Estimated arrival times for sample B2 are shown in Figure 4. From the changes in the first arrivals, we estimate an average increase in *P* wave velocity from 0 to 15 weeks of 5%, 5%, and 10% for samples B1, B2, and B3, respectively. An additional increase in velocity from 15 to 30 weeks is 8%, 4%, and 12%, respectively.

[17] The *P* wave is followed by a sequence of waves, often referred to as *coda* waves. These include contributions from (body) waves scattered by internal heterogeneity but are often dominated by (scattered) evanescent waves propagating along the surface of the sample. These surface waves are most sensitive to the shear wave properties of the medium [*Aki and Richards*, 2002]. To quantify changes in the coda, wave fields are first band-pass filtered (80–90 kHz)
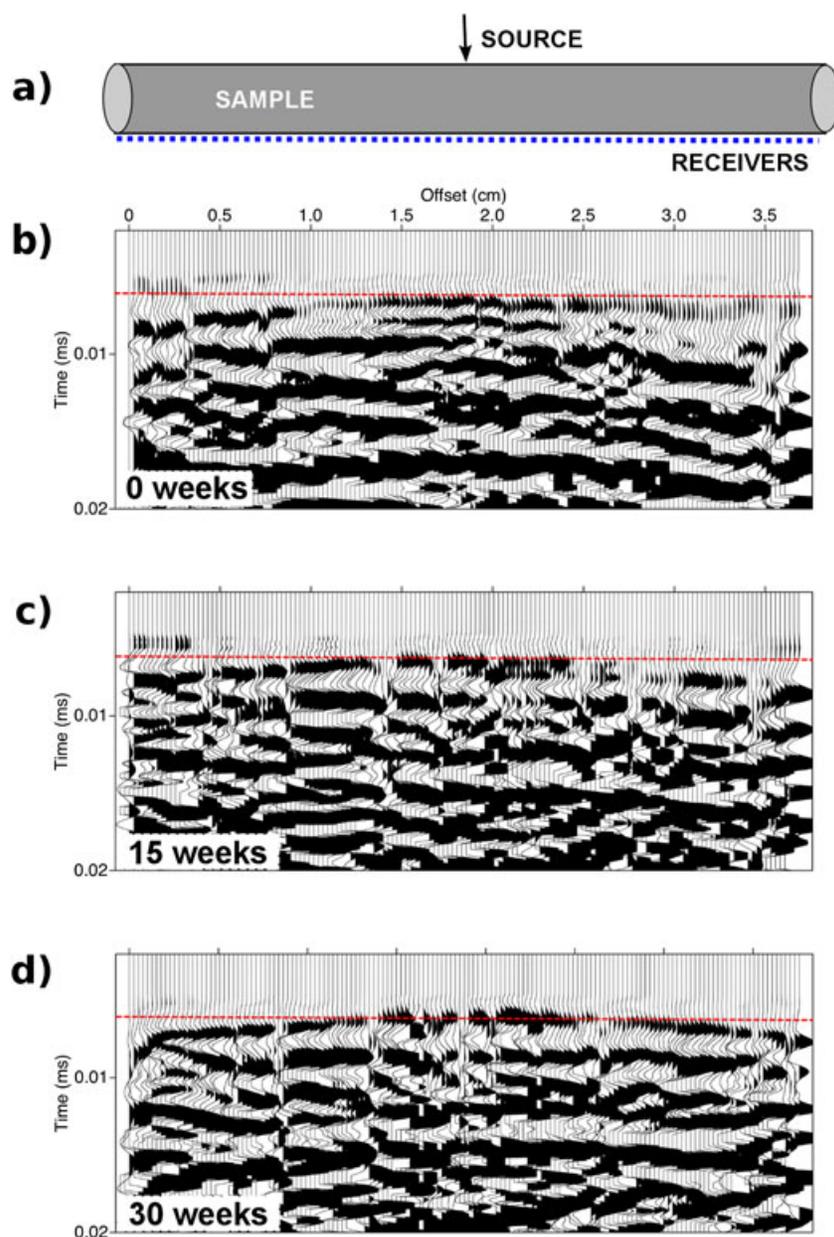
Figure 3. Ultrasonic wave forms on basalt B2. (a) The experimental geometry. Elastic wave fields (b) before rock-fluid interactions, (c) after 15 weeks, and (d) after 30 weeks of rock-fluid reactions. Each vertical wiggle trace represents the wave field at a particular receiver location. The first (*P* wave) arrival time decreases with respect to a reference horizontal red line drawn at $t = 0.005$ ms.

and then cross-correlated in time windows of the entire recording. As the travel time increases, these waves sample the rock increasingly well and prove sensitive to small changes in the elastic properties. This technique called coda wave interferometry has been successfully applied to monitor changes in volcanoes [e.g., *Grêt et al.*, 2005]. Common phases of filtered wave forms in Figure 5 show that seismic speed increases after rock-fluid interactions. On average, the shear wave speed increases by 0.9%, 1.4%, and 1.6% (for the 0–15 week period), and 2.2%, 1.7%, and 1.7% (for the 15–30 week period) for basalts B1, B2, and B3, respectively. The absolute values of ultrasonic wave velocities in these basalt samples (dry and fluid-saturated) are described in *Adam and Otheim* [2013].

5. Evidence of Carbonate Formation

[18] To correlate changes in the ultrasonic data with changes in the rock frame, we repeat our petrographical analyses and introduce water chemistry results. Thin sections of the samples after the rock-fluid interactions also display changes (Figures 1d–1h). The mineral precipitation in the vesicles and cracks of our basalt samples (shown enlarged in the right panels of Figure 1) are most likely carbonates because of (1) the rounded (botryoidal) habit of the minerals lining the vesicle, (2) the high relief observed in the plain polarized light—with distinct variations in relief as the stage is rotated, and (3) the extreme interference colors observed in the cross-polarized light. The thin sections also indicate
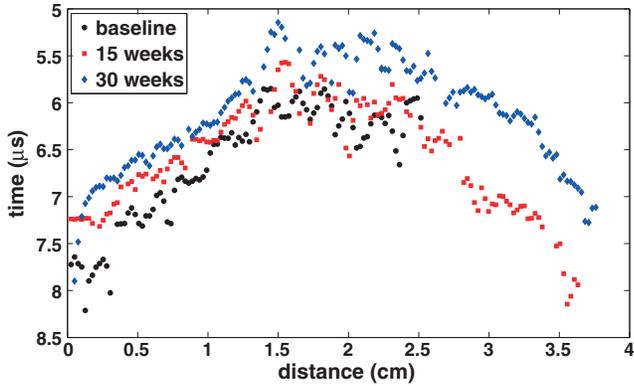
Figure 4. *P* wave arrival times for ultrasonic wave transmission in sample B2. The observed changes are not equal for all receiver positions, suggesting that changes vary within the sample. An average velocity is estimated from this plot (and similar ones for samples B1 and B3), and the results of the average velocity changes per sample are summarized in Table 1.
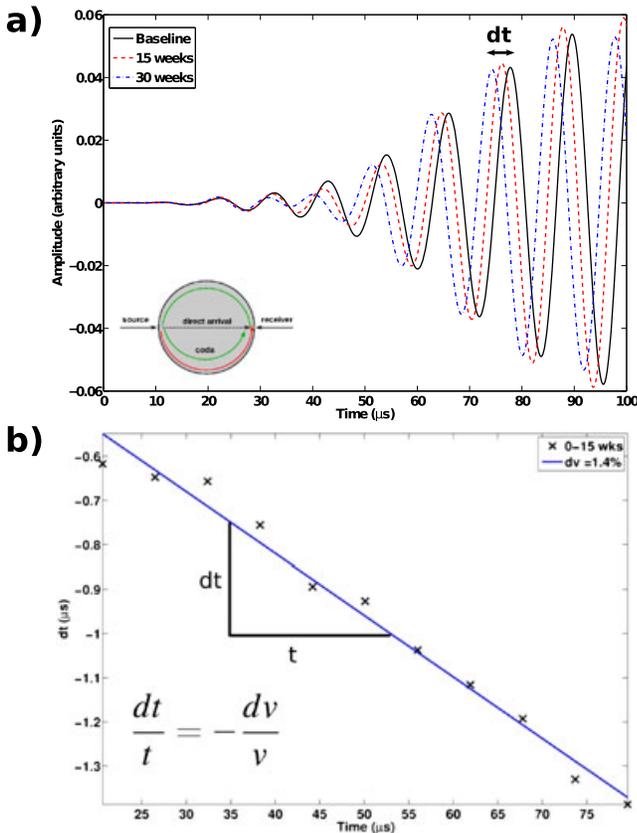

Figure 5. Coda wave analysis. (a) Filtered wave forms for one source-receiver pair in sample B2, after 0, 15, and 30 weeks of rock-fluid interactions. The relative time shift (d*t*) between common phases increases with recording time *t*. (b) Time shifts estimated from cross correlation of 0 and 15 week traces, averaged for all the recorded traces in sample B2. The slope of this line is inversely proportional to the change in wave speed.
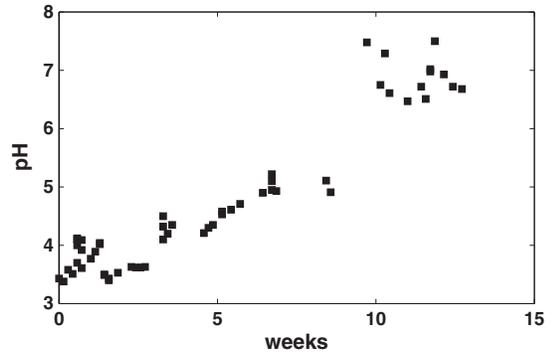

Figure 6. pH of the CO_2-water solution in the reactor vessel for the first 13 weeks of rock-fluid interactions. The reactor pressure is at 8.3 MPa, and the temperature is 100°C. The significant increase in pH toward a more basic solution is indicative of an increase in metal cations (i.e., mineral dissolution) in the solution.

that the dissolved cations initially come from the groundmass, because olivine, pyroxene, and plagioclase show little signs of alteration.

[19] The thin sections are partly stained with Alizarin Red (pink-for calcite) and K-ferricyanide (blue for Mg, Fe minerals) to assist in mineral identification. Figure 1h shows a high-resolution thin section with a botryoidal precipitate that mostly absorbed K-ferricyanide, suggesting this is an iron/magnesium carbonate. The availability of such metal cations is supported by water chemistry and pH levels introduced next.

[20] Figure 6 depicts the pH of the water-CO_2 mixture in the pressure vessel from 0 to 13 weeks, where pressure is 8.3 MPa and temperature is 100°C. Initially, the pH is that of a water-CO_2 mixture at high pressure and temperature ($\sim$ 3.2 [*Meyssami et al.*, 1992]). Basalt dissolution leaches cations into the aqueous solution [*McGrail et al.*, 2006; *Schaef and McGrail*, 2009]. As carbonates start precipitating by consuming cations in the solution, the pH of the solution increases. This is supported by elemental concentration in the reactor water. The high-pressure pH probe stopped working after 13 weeks, and thus the solution pH for the 13–30 week interval was not recorded.

[21] We study the elemental concentration in (1) water with crushed basalt at room conditions (baseline) and (2) water extracted from the reactor vessel after the 30 weeks of rock-fluid interactions. The element concentration of the baseline water is shown in the top panel of Figure 7. During the first 2 weeks there is a significant increase in cations as basalt and water equilibrate. The equilibrated baseline water—resembling formation water—is the input water for the rock-fluid interactions. The bottom panel of Figure 7 is a comparison of the metal cations after 15 and 30 weeks in the baseline water to the water extracted from the reactor at the same times. Compared to the baseline water, the element concentration in the reactor water increases 2 orders of magnitude on dissolved [25]Mg, [57]Fe, and [55]Mn, with lower concentration of [44]Ca and [29]Si. Based on the availability of magnesium and iron in the vessel water and the observations on thin sections, we interpret that some of the carbonate precipitate is of Fe-Mg composition.
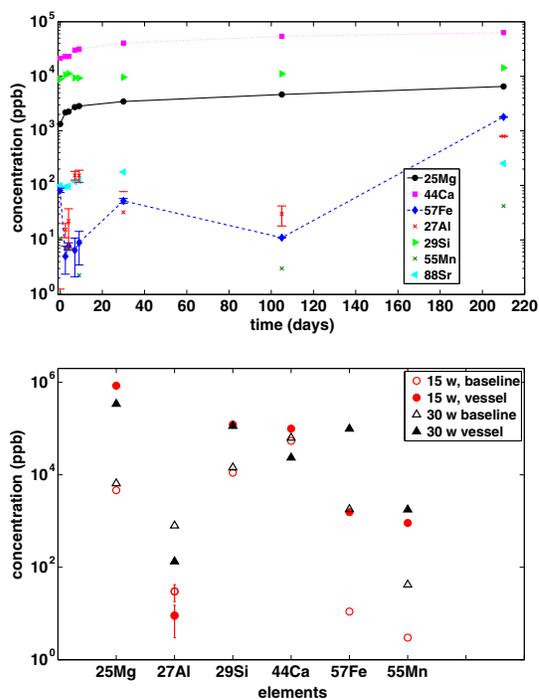
Figure 7. Water chemistry of the reactor and baseline water. (top) Element concentration in the baseline water, due to basalt dissolution in tap water at room conditions, as a function of time. The largest mineral dissolution occurs in the first 2 weeks of the water-basalt equilibration. (bottom) Concentration of metal cations in the reactor water at 15 and 30 weeks (solid symbols) compared to baseline water (open symbols). The significant disparities are in ^{25}Mg, ^{57}Fe, and ^{55}Mn.

Table 4. Loss on Ignition (LOI) Measures Mass Changes as a Function of Temperature[a]

LOI %	Before	After
B1	−1.55	0.42
B2	−0.59	0.56
B3	−1.06	0.46

[a]Carbonates can be burned creating a loss of mass, while oxidation will result in a mass gain.

[23] Thin section point counts indicate that the volume of precipitated carbonates is between 1% and 1.5% of the total mineral volume in the samples. The porosity of the rock estimated from CT-scan data varies by 1–2% before and after reactions. Both of these estimates overall agree with a 1–2.5% increase in mineral volume estimated from the helium pycnometry measurements before and after reaction (Table 1). XRD measurements on the samples after reactions do not indicate a presence of carbonates, because the mineral volume of formed carbonates (1–1.5%) is below the XRD resolution threshold.

[24] CT-scan images after carbonate precipitation show that carbonates have not filled large volumes of pores (Figure 2). Only localized areas of these whole-rock images, highlighted by arrows, contain secondary (carbonate) precipitation. This agrees with the changes in porosity estimated from pycnometry, suggesting that less than 2% volume of secondary minerals have precipitated. CT-scan images in Figures 2g and 2h sample the basalts after carbonate precipitation at a higher resolution. In these, carbonates are identified in pores and cracks and have botryoidal texture as observed in the thin sections.

[25] The XRF analyses before and after mineralization are summarized in Table 3, but the samples sent for analysis ($\sim$ 1 cm^3) may have been too small to be representative of the rocks as a whole. As a result, the observed changes could come from a higher ratio of groundmass in the reacted sample, which result in greater values for Fe and Ti, while unreacted samples may have contained more plagioclase, olivine, and pyroxene crystals, which would result in greater values for Ca, Al, and Mg. However, the loss on ignition (LOI) test in the Table 4 experiment can be indicative of carbonates. All three samples after 30 weeks have a loss of mass when heated to 950°C, meaning that some portion of the sample was volatile. *Heiri et al.* [2001] show that in the presence of carbonates, when a rock sample is significantly heated, carbonates become volatile. LOI performed on the baseline samples actually led to a mass gain due to an oxidation reaction.

[22] The permeability and porosity of these basalt samples decrease after 30 weeks of rock-fluid interactions (Table 1). Permeability decreases by 0.5 to 1 order of magnitude for basalts B1 and B3, respectively, while sample B2 was unable to support any fluid flow after reactions. Fractures control the rock permeability, and for basalts these mostly result from the cooling process. This suggests that fractures in these samples are obstructed by the newly formed carbonate minerals. Figures 1d and 1g show such cracks with carbonate growth at four locations along the fractures. Mineralization blocking a larger pore is shown in Figures 1e and 1h.

Table 3. The XRF Analysis of the Basalt Samples Confirm Similarity in Chemical Composition in Terms of Weight Percentage[a]

Oxides %	SiO_2	Al_2O_3	Fe_2O_3	CaO	MgO	Na_2O	TiO_2	K_2O	MnO	P_2O_5
B1$_0$	46.34	15.38	15.55	9.28	6.91	2.59	2.93	0.70	0.20	0.70
B1$_{30}$	44.72	13.67	19.65	8.64	5.96	2.40	3.41	0.81	0.25	0.77
B2$_0$	45.98	13.36	16.72	9.05	6.73	2.45	3.57	0.86	0.22	0.91
B2$_{30}$	44.75	13.02	17.92	8.87	6.94	2.35	3.51	0.76	0.24	0.73
B3$_0$	45.82	14.36	16.70	9.24	6.76	2.51	3.32	0.77	0.21	0.81
B3$_{30}$	45.44	14.30	16.58	8.91	6.57	2.45	3.46	0.75	0.22	0.76

[a]Values are obtained before (0) and after (30 weeks) of CO_2-basalt reactions.

6. Discussion

[26] Ultrasonic waves proved sensitive to changes in basalts due to 30 weeks of exposure to CO_2 and water. Carbonate precipitation in pores and cracks resulted in wave speeds increasing by 4% to 20%, even though petrographical analyses indicated that the total volumetric contribution of these carbonates reached only 1–2%. However, permeability decreased by 0.5 to 1 order of magnitude after basalt-CO_2 reactions. *Grombacher et al.* [2012] measure carbonate rocks exposed to CO_2 and observe a similar correlation between large changes in velocity and permeability but much smaller changes in porosity.

[27] The compliance of rock fractures and pores are important in the characteristics of elastic wave propagation. As carbonates precipitated in these cracks and pores, the rock stiffened and its wave speed increased. The observed reduction in permeability due to fracture blockage is in agreement with observations of a significant increase in wave speed before and after carbonic acid-basalt reactions. This holds especially true for basalt B3, for which the largest changes in velocity, permeability, and porosity and in CT-scan images were observed.

[28] The reaction experiment was stopped at 30 weeks. How long the dissolution of basalt and carbonate precipitation could have continued depends on the availability of CO_2 and the rock-fluid reactivity kinetics, among other parameters. Recently, *Schaef et al.* [2013] have shown data on basalt reactivity with CO_2 and H_2S lasting 3.5 years.

[29] Although this data set was limited in size, correlation between rock mineralogy and carbonate precipitation has not been observed. Samples B1 and B3 were almost identical in mineral composition and chemistry; nonetheless, sample B3 showed the larger changes in wave velocity and permeability, probably controlled by the pore microstructure. While sample B2 was mineralogically different from B1 (B2 had no glass) the changes in velocity were similar among these samples. Altogether, the volume of carbonate precipitate was less than 2%, but the changes in velocity were significant and could potentially be observed in the field with borehole seismic methods [*Khatiwada et al.*, 2012].

[30] This study showed that the elastic properties of the rock frame change when CO_2 is injected into the reservoir. *Lumley* [2010] discusses how changes in time-lapse seismic surface data in CO_2 injection scenarios in sedimentary basins cannot always be described by current elastic rock-physics models. This is because rock-fluid reactions change the rock frame, while most rock-physics models only account for fluid substitution or the closure of cracks with pressure [e.g.,*Gassmann*, 1951; *Kuster and Toksöz*, 1974].

[31] Recently, changes to the permeability and elasticity of the rock frame due to CO_2-water-rock reactions have been measured in sedimentary rocks in the laboratory. Rock frame weakening has been observed due to carbonate mineral dissolution in limestones [*Grombacher et al.*, 2012; *Vialle and Vanorio*, 2011; *Mohamed et al.*, 2012] and sandstone [*Joy et al.*, 2011] and due to chlorite and siderite dissolution in shale [*Armitage et al.*, 2013]. Brine alone has been also shown to weaken the rock frame of carbonate rocks [*Adam et al.*, 2006]. However, secondary mineral precipitation has also been observed by *Vanorio et al.* [2011], where CO_2 can induce salt precipitation in brine-saturated sandstones.

These studies of rock-fluid interactions, and the work presented here, demonstrate that the assumption of a constant elastic rock frame, common in most elastic rock-physics theories, might not hold true for fluid substitution with CO_2. Ignoring the effect of rock-CO_2 reactivity might bias the interpretation of time-lapse changes in seismic data.

[32] Close to the CO_2 injection site the fluid mixture will flow, but as the CO_2 plume diffuses, it might reach geologic constraints (traps) that would limit its mobility. In our experiments there is no fluid movement in the system, resembling a geologic trap in the subsurface. In this scenario, carbonate precipitation strengthens the basalt frame and blocks permeability paths. However, to represent subsurface fluids flow, future studies are needed to understand the balance between carbonate precipitation and the potential dissolution (due to carbonic acid) of these newly formed carbonates.

7. Conclusions

[33] Experiments of CO_2-water-basalt reactions show that the rock frame in basalt samples stiffens as a result of carbonate precipitation in rock fractures and pores. After 30 weeks of reactions the volume of newly formed carbonate minerals is 1–2% of the total mineral volume. Nonetheless, *P* and *S* wave velocity increase by 9–22% and 3%, respectively. Combined with a rock permeability decrease of 0.5 to 1 order of magnitude, this suggests that precipitation dominantly occurs in fractures and compliant pores.

[34] Our study of CO_2-basalt reactivity has two important implications. First, this study presents evidence that secondary mineral precipitation introduces elastic changes that can potentially be monitored in the field with elastic waves (although we recognize that massive basalts still form challenging conditions for seismic imaging). Second, changes in seismic wave speed cannot be explained with existing fluid substitution only, as mineralization clearly affected the rock frame.

References

Adam, L., and T. Otheim (2013), Elastic laboratory measurements and modeling of saturated basalts, *J. Geophys. Res. Solid Earth*, *118*(3), 840–851, doi:10.1002/jgrb.50090.

Adam, L., M. Batzle, and I. Brevik (2006), Gassmann's fluid substitution and shear modulus variability in carbonates at laboratory seismic and ultrasonic frequencies, *Geophysics*, *71*(6), F173–F183, doi:10.1190/1.2358494.

Adelinet, M., J. Fortin, Y. Guéguen, A. Schubnel, and L. Geoffroy (2010), Frequency and fluid effects on elastic properties of basalt: Experimental investigations, *Geophys. Res. Lett.*, *37*, L02303, doi:10.1029/2009GL041660.

Aki, K., and P. G. Richards (2002), *Quantitative Seismology* (2nd edn), Univ. Science Books, Sausalito, CA.

Armitage, P., D. Faulkner, and R. Worden (2013), Caprock corrosion, *Nat. Geosci.*, *6*(2), 79–80.

Arts, R., O. Eiken, A. Chadwick, P. Zweigel, L. van der Meer, and B. Zinszner (2004), Monitoring of CO_2 injected at Sleipner using time-lapse seismic data, *Energy*, *29*(9–10), 1383–1392, doi:10.1016/j.energy.2004.03.072.

Bachu, S. (2003), Screening and ranking of sedimentary basins for sequestration of CO_2 in geological media in response to climate change, *Environ. Geol.*, *44*(3), 277–289.

Bachu, S., W. Gunter, and E. Perkins (1994), Aquifer disposal of CO_2: Hydrodynamic and mineral trapping, *Energy Convers. Manage.*, *35*(4), 269–279, doi:10.1016/0196-8904(94)90060-4.

Baker, L. L., D. J. Agenbroad, and S. A. Wood (2000), Experimental hydrothermal alteration of a martian analog basalt: Implications for Martian meteorites, *Meteorit. Planet. Sci.*, *35*(1), 31–38.

Benson, S. M., and D. R. Cole (2008), CO_2 sequestration in deep sedimentary formations, *Elements*, *4*, 325–331.

Blum, T., K. van Wijk, B. Pouet, and A. Wartelle (2010), Multicomponent wavefield characterization with a novel scanning laser interferometer, *Rev. Sci. Instrum.*, *81*(7), 073,101–073,101.

Bruhn, R. L., W. T. Parry, W. A. Yonkee, and T. Thompson (1994), Fracturing and hydrothermal alteration in normal fault zones, *Pure Appl. Geophys.*, *142*, 609–644.

Caine, J. S., R. L. Bruhn, and C. B. Forster (2010), Internal structure, fault rocks, and inferences regarding deformation, fluid flow, and mineralization in the seismogenic stillwater normal fault, Dixie Valley, Nevada, *J. Struct. Geol.*, *32*(11), 1576–1589, doi:10.1016/j.jsg.2010.03.004.

Daley, T. M., E. L. Majer, and J. E. Peterson (2004), Crosswell seismic imaging in a contaminated basalt aquifer, *Geophysics*, *69*(1), 16–24.

Eaton, D., S. Guest, B. Milkereit, W. Bleeker, D. Crick, D. Schmitt, and M. H. Salisbury (1996), Seismic imaging of massive sulfide deposits: Part III, borehole seismic imaging of near-vertical structures, *Econ. Geol.*, *91*(5), 835–840.

Gassmann, F. (1951), Über die elastizität poröser medien, *Viertel. Naturforsch. Ges. Zürich*, *96*, 1–23.

Giammar, D. E., R. G. Bruant Jr., and C. A. Peters (2005), Forsterite dissolution and magnesite precipitation at conditions relevant for deep saline aquifer storage and sequestration of carbon dioxide, *Chem. Geol.*, *217*(34), 257–276, doi:10.1016/j.chemgeo.2004.12.013.

Gislason, S. R., and P. E. Hans (1987), Meteoric water-basalt interactions. I: A laboratory study, *Geochim. Cosmochim. Acta*, *51*(10), 2827–2840, doi:10.1016/0016-7037(87)90161-X.

Gislason, S. R., and E. H. Oelkers (2003), Mechanism, rates, and consequences of basaltic glass dissolution: II. An experimental study of the dissolution rates of basaltic glass as a function of ph and temperature, *Geochim. Cosmochim. Acta*, *67*(20), 3817–3832.

Gislason, S. R., et al. (2010), Mineral sequestration of carbon dioxide in basalt: A pre-injection overview of the Carbfix project, *Int. J. Greenhouse Gas Control*, *4*(3), 537–545, doi:10.1016/j.ijggc.2009.11.013.

Goldberg, D. (2011), Volcanology: Carbon below the sea floor, *Nat. Geosci.*, *4*(1), 11–12, doi:10.1038/ngeo1019.

Grêt, A., R. K. Snieder, R. C. Aster, and P. R. Kyle (2005), Monitoring rapid temporal change in a volcano with coda wave interferometry, *Geophys. Res. Lett.*, *32*, L06304, doi:10.1029/2004GL021143.

Grombacher, D., T. Vanorio, and Y. Ebert (2012), Time-lapse acoustic, transport, and NMR measurements to characterize microstructural changes of carbonate rocks during injection of CO2-rich water, *Geophysics*, *77*(3), WA169–WA179, doi:10.1190/geo2011-0281.1.

Heiri, O., A. F. Lotter, and G. Lemcke (2001), Loss on ignition as a method for estimating organic and carbonate content in sediments: Reproducibility and comparability of results, *J. Paleolimnol.*, *25*(1), 101–110.

Johnston, J., and N. Christensen (1997), Seismic properties of layer 2 basalts, *Geophys. J. Int.*, *128*(2), 285–300.

Joy, C., T. Vanorio, and M. K. Sen (2011), Differentiating chemical effects and pressure effects on the elastic properties of the lower Tuscaloosa sandstone in Cranfield, Mississippi by injecting carbon dioxide rich brine, in *2011 SEG Annual Meeting*.

Kelley, D. S., et al. (2001), An off-axis hydrothermal vent field near the Mid-Atlantic ridge at 30°N, *Nature*, *412*, 145–149, doi:10.1038/35084000.

Khatiwada, M., L. Adam, M. Morrison, and K. van Wijk (2012), A feasibility study of time-lapse seismic monitoring of CO_2 sequestration in a layered basalt reservoir, *J. Appl. Geophys.*, *82*(0), 145–152, doi:10.1016/j.jappgeo.2012.03.005.

Kuster, G. T., and M. N. Toksöz (1974), Velocity and attenuation of seismic waves in two-phase media: Part I. Theoretical formulations, *Geophysics*, *39*(5), 587–606, doi:10.1190/1.1440450.

Landrø, M. (2001), Discrimination between pressure and fluid saturation changes from time-lapse seismic data, *Geophysics*, *66*(3), 836–844.

Lopez, D. L., and S. N. Williams (1993), Catastrophic volcanic collapse: Relation to hydrothermal processes, *Science*, *260*, 1794–1796.

Lumley, D. (2010), 4D seismic monitoring of CO_2 sequestration, *Leading Edge*, *29*(2), 150–155.

Matter, J. M., and P. B. Kelemen (2009), Permanent storage of carbon dioxide in geological reservoirs by mineral carbonation, *Nat. Geosci.*, *2*(12), 837–841, doi:10.1038/ngeo683.

Matter, J. M., T. Takahashi, and D. Goldberg (2007), Experimental evaluation of in situ CO_2-water-rock reactions during CO_2 injection in basaltic rocks: Implications for geological CO_2 sequestration, *Geochem. Geophys. Geosyst.*, *8*, Q02001, doi:10.1029/2006GC001427.

McGrail, B., F. Spane, E. Sullivan, D. Bacon, and G. Hund (2011), The Wallula basalt sequestration pilot project, *Energy Procedia*, *4*(0), 5653–5660, doi:10.1016/j.egypro.2011.02.557.

McGrail, B. P., H. T. Schaef, A. M. Ho, Y.-J. Chien, J. J. Dooley, and C. L. Davidson (2006), Potential for carbon dioxide sequestration in flood basalt, *J. Geophys. Res.*, *111*, B12201, doi:10.1029/2005JB004169.

Meyssami, B., M. O. Balaban, and A. A. Teixeira (1992), Prediction of pH in model systems pressurized with carbon dioxide, *Biotechnol. Progr.*, *8*(2), 149–154.

Mohamed, I., J. He, and H. Nasr-El-Din (2012), Carbon dioxide sequestration in sandstone aquifers: How does it affect the permeability? *Carbon Management Technology Conference*, Orlando, Fla.

Oelkers, E. H., S. R. Gislason, and J. Matter (2008), Mineral carbonation of CO_2, *Elements*, *4*(5), 333–337, doi:10.2113/gselements.4.5.333.

Pujol, J., and S. Smithson (1991), Seismic wave attenuation in volcanic rocks from VSP experiments, *Geophysics*, *56*(9), 1441–1455.

Reid, M. E., T. W. Sisson, and D. L. Brien (2001), Volcano collapse promoted by hydrothermal alteration and edifice shape, Mount Rainier, Washington, *Geology*, *29*(9), 779–782, doi:10.1130/0091-7613(2001)029<0779:VCPBHA>2.0.CO;2.

Romanek, C., M. Grady, I. Wright, D. Mittlefehldt, R. Socki, C. Pillinger, and E. Gibson (1994), Record of fluid rock interactions on Mars from the meteorite ALH84001, *Nature*, *372*(6507), 655–657.

Saar, M. O., and M. Manga (1999), Permeability-porosity relationship in vesicular basalts, *Geophys. Res. Lett.*, *26*(1), 111–114.

Schaef, H. T., and B. P. McGrail (2009), Dissolution of Columbia River Basalt under mildly acidic conditions as a function of temperature: Experimental results relevant to the geological sequestration of carbon dioxide, *Appl. Geochem.*, *24*(5), 980–987, doi:10.1016/j.apgeochem.2009.02.025.

Schaef, H. T., B. P. McGrail, and A. T. Owen (2010), Carbonate mineralization of volcanic province basalts, *Int. J. Greenhouse Gas Control*, *4*(2), 249–261.

Schaef, H. T., B. P. McGrail, A. T. Owen, and B. W. Arey (2013), Mineralization of basalts in the CO_2-H_2O-H_2S system, *Int. J. Greenhouse Gas Control*, *16*, 187–196.

Torp, T. A., and J. Gale (2004), Demonstrating storage of CO_2 in geological reservoirs: The Sleipner and SACS projects, *Energy*, *29*(9–10), 1361–1369, doi:10.1016/j.energy.2004.03.104, 6th International Conference on Greenhouse Gas Control Technologies.

Tura, A., and D. E. Lumley (1998), Subsurface fluid flow properties from time-lapse elastic wave reflection data, in *SPIE's International Symposium on Optical Science, Engineering, and Instrumentation*, pp. 125–138, International Society for Optics and Photonics, San Diego, Calif., doi:10.1117/12.323284.

Vanorio, T., M. Prasad, D. Patella, and A. Nur (2002), Ultrasonic velocity measurements in volcanic rocks: Correlation with microtexture, *Geophys. J. Int.*, *149*(1), 22–36.

Vanorio, T., J. Virieux, P. Capuano, and G. Russo (2005), Three-dimensional seismic tomography from P wave and S wave microearthquake travel times and rock physics characterization of the Campi Flegrei Caldera, *J. Geophys. Res.*, *110*, B03201, doi:10.1029/2004JB003102.

Vanorio, T., A. Nur, and Y. Ebert (2011), Rock physics analysis and time-lapse rock imaging of geochemical effects due to the injection of CO_2 into reservoir rocks, *Geophysics*, *76*(5), O23–O33, doi:10.1190/geo2010-0390.1.

Vialle, S., and T. Vanorio (2011), Laboratory measurements of elastic properties of carbonate rocks during injection of reactive CO_2-saturated water, *Geophys. Res. Lett.*, *38*, L01302, doi:10.1029/2010GL045606.

Wolff-Boenisch, D., S. R. Gislason, and E. H. Oelkers (2006), The effect of crystallinity on dissolution rates and CO_2 consumption capacity of silicates, *Geochim. Cosmochim. Acta*, *70*(4), 858–870.

Zandomeneghi, D., A. Barclay, J. Almendros, J. M. I. Godoy, W. S. Wilcock, and T. Ben-Zvi (2009), Crustal structure of deception island volcano from p wave seismic tomography: Tectonic and volcanic implications, *J. Geophys. Res.*, *114*, B06310, doi:10.1029/2008JB006119.